International Journal of Nanomedicine

Dovepress
open access to scientific and medical research

Open Access Full Text Article

ORIGINAL RESEARCH

Experimental Investigation of Temperature Influence on Nanoparticle Adhesion in an Artificial Blood Vessel

Kai Yue[1,2], Chao Yang[1], Yu You[1,2], Xueying Wang[3], Xinxin Zhang[1]

[1]School of Energy and Environmental Engineering, University of Science and Technology Beijing, Beijing, 100083, People's Republic of China; [2]Shunde Graduate School of University of Science and Technology Beijing, Shunde, Guangdong Province, 528399, People's Republic of China; [3]School of Chemistry and Chemical Engineering, University of Jinan, Jinan, Shandong Province, 250022, People's Republic of China

Correspondence: Kai Yue, Email yuekai@ustb.edu.cn

Background: A good understanding of the adhesion behaviors of the nanocarriers in microvessels in chemo-hyperthermia synergistic therapy is conducive to nanocarrier design for targeted drug delivery.

Methods: In this study, we constructed an artificial blood vessel system using gelatins with a complete endothelial monolayer formed on the inner vessel wall. The numbers of adhered NPs under different conditions were measured, as well as the interaction forces between the arginine–glycine–aspartic acid (RGD) ligands and endothelial cells.

Results: The experimental results on the adhesion of ligand–coated nanoparticles (NPs) with different sizes and morphologies in the blood vessel verified that the gelatin-based artificial vessel possessed good cytocompatibility and mechanical properties, which are suitable for the investigation on NP adhesion characteristics in microvessels. When the temperature deviated from 37 °C, an increase or decrease in temperature resulted in a decrease in the number of adhered NPs, but the margination probability of NP adhesion increased at high temperatures due to the enhanced Brownian movement and flow disturbance. It is found that the effect of cooling was less than that of heating according to the observed changes in cell morphology and a decrease in cell activity under the static and perfusion culture conditions within the temperature range of 25 °C–43 °C. Furthermore, the measurement results of change in the RGD ligand-cell interaction with temperature showed good agreement with those in the number of adhered NPs.

Conclusion: The Findings suggest that designing ligands that can bind to the receptor and are least susceptible to temperature variation can be an effective means to enhance drug retention.

Keywords: artificial vessel, drug delivery, nanoparticle, temperature variation, particle–wall adhesion

Introduction

Nanoparticle (NP)-mediated drug delivery has been proven to have the potential for increasing the efficiency of the diagnosis and treatment of target lesions.[1–3] Various nanocarriers modified with different ligands are being widely investigated and developed to enrich the amount of diagnostic/therapeutic agents in target areas and reduce side effects.[4–6] In recent years, synergistic therapy that combines NP-mediated drug delivery and the action of external fields, such as phototherapy, thermal therapy, and electromagnetic therapy, has attracted attention as a promising approach to improve targeted drug delivery and release.[7,8] The temperature of treated tissues is generally changed under the influence of external fields. After nanocarriers are injected into a subject, the behaviors of NP transport in blood vessels and NP adhesion on vessel walls are evidently influenced by the NP properties and microenvironment temperature.[9–11]

The physical properties of NPs play important roles in NP transport and adhesion in blood vessels. Previous studies have shown that small spheres tend to adhere to the wall because the Brownian force acting on the NPs dominates over the gravity force with the decrease in particle diameter.[12–14] Compared with 100 or 200 nm polystyrene spheres, 50 nm spheres marginated more significantly in a flow channel made from polymethyl methacrylate (PMMA) and cultured with human umbilical vein endothelial cells (HUVECs).[15] Small liposomes NPs with diameters of 65–130 nm move to the

Received: 21 November 2022
Accepted: 17 January 2023
Published: 22 January 2023

wall of a microfluidic chamber due to fast Brownian motion.[16] NP shape is another crucial factor that influences NP transport.[17,18] Studies have found that nanorods are more likely to be internalized by HeLa cells through several mechanisms of endocytosis[19] and exhibit higher deposition than spheres.[20] Non-spherical polymer micelles display enhanced margination and can persist in the circulation up to more than one week after intravenous injection.[21,22] In the different stages of particle transport, the optimal size and shape of the NPs is different, therefore it is necessary to investigate the size and shape effect of the NPs on the interaction between NPs and tissues.[23,24] Moreover, various materials and external stimuli have been widely investigated for their effects on drug delivery, including gold NPs,[25,26] silver NPs,[27,28] porous silica NPs,[29,30] liposome NPs,[31,32] temperature,[33] magnetic field,[34] and ultrasonic.[35] NPs coated with ligand molecules can bind specifically to the endothelial surface for targeted drug delivery.[36–38] Previous studies have reported receptor-targeted delivery systems utilizing ICAM-1 and ICAM-1 specific antibodies to increase the binding rate of carrier particles.[39,40] Ferritin coated with RGDs can also effectively target tumor tissues via the interaction between RGDs and integrins.[41,42]

Furthermore, attempts have been made to enhance NP deposition, cellular uptake, and intracellular drug release by thermal, electric, magnetic, optical, and acoustic activation. Studies have shown that the deposition of ferrimagnetic NPs in tumor tissues can improve the treatment efficiency of microwave ablation.[43,44] In a previous research, gold NPs were utilized as thermal sensitizers to absorb radio frequency radiation power and increase heating efficiency.[45] The gold–silicon nanoshells were injected into mice, and continuous diode laser irradiation effectively reduced the tumor symptoms because of the strong near-infrared (NIR) absorption.[46] In addition, MR-guided focused ultrasound can reversibly disrupt the blood–brain barrier and facilitate the delivery of polystyrene NPs.[47] Notably, the application of external fields is commonly accompanied with changes in the temperature of treated tissues, which may affect NP transport and NP–cell interactions. Generally, the experimental research on the transport and adhesion behaviors of NPs is commonly carried out in an artificial blood vessel.[48,49] However, up to now, no study has examined the thermal effect caused by an external field on NP adhesion in simulated blood vessels. In addition, the majority of existing experimental studies that used microchannel technology are based on parallel plate flow chambers or microchannels composed of PMMA[22] or polydimethylsiloxane (PDMS)[16] with avidin, fibronectin or type I collagen from rat tail covered on the surface of the simulated microvessel. The mechanical elasticity and permeability of an artificial vessel wall, which are sensitive to flow stress, should be similar to those of a real vessel wall as much as possible to facilitate the activity and growth of endothelial cells under continuous perfusion.

The objective of this study is to construct an artificial vessel system to investigate the effects of NP properties and environmental temperature on NP transport and adhesion characteristics in a microvessel with a blood flow. A gelatin-based material was applied to fabricate the vessel, and HUVEC cells were covered on the inner surface of the vessel. Then, a corresponding experimental system was developed to simulate the blood flow and NP adhesion in real vessels. Under static and perfusion culture conditions, the effects of temperature and blood flow on the morphology and activity of the HUVEC cells were observed and analyzed. The adhesion characteristics of arginine–glycine–aspartic acid (RGD)-modified NPs with different sizes and shapes on the vessel wall were explored under different temperatures. Moreover, the interaction forces between RGD ligands and receptors on HUVEC cells were measured for further analysis of temperature influence on NP adhesion.

Materials and Methods

System

Figure 1 shows the constructed experimental system, which consisted of an artificial blood vessel, a microsyringe pump (PhD ultra 70–3007, HARVARD, USA), a temperature control unit, an inverted fluorescence microscope, and an inductively coupled plasma-mass spectrometry instrument (ICP-MS). Human whole blood was pumped into the vessel to simulate the blood flow in microvessels. After reaching steady-state flow conditions, the NP suspension was injected into the whole blood, and then pumped into the vessel. The temperature unit, including a thermostatic water bath and a solid-state plug-in stage, was employed to provide constant-temperature circulating flow in the vessel. During the 1 h of perfusion with the mixture of the whole blood and NP suspension through the vessel, the inverted fluorescence

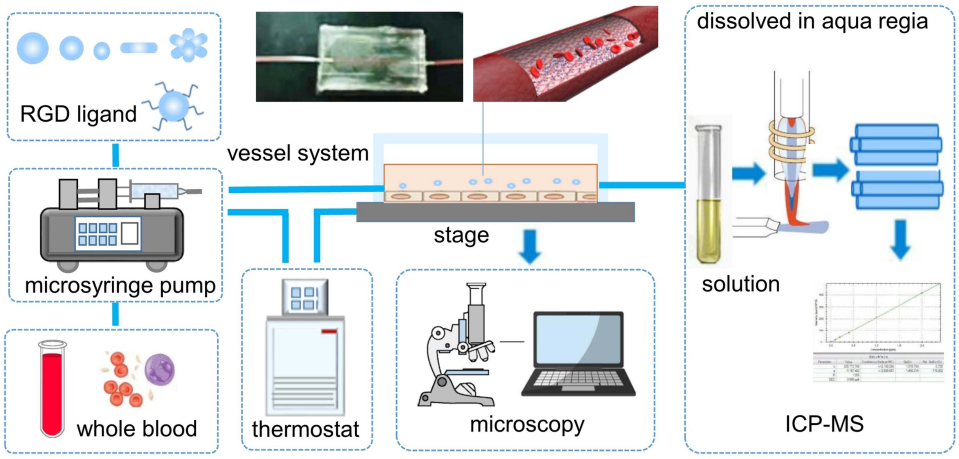

Figure 1 Sketch of the experimental system. The solution (109 particles/mL) of RGD ligand-modified gold NPs with different shapes and sizes was mixed with the whole-blood (106 cells/mL) and then was injected into an artificial blood vessel, which was covered with a layer of endothelial cells on the inner surface. An inverted fluorescence microscope and an ICP-MS detector were used to observe the cells and to measure the number of adhered NPs at the temperatures of 25°C, 37°C, 39°C, 41°C and 43°C.

microscope was used to monitor the experiment and observe the changes in the endothelium cells on the inner wall of the vessel. Then, the NP adhesion in the vessel was quantitatively characterized via the ICP-MS.

Gelatin-Based Artificial Blood Vessel

Gelatin was employed to fabricate the artificial blood vessels because of its excellent biocompatibility that allows endothelial cells to grow well in the channels; it also has good permeability, mechanical elasticity, and temperature sensitivity. Specifically, 2.5 g of gelatin and 0.2 g of glutamine transaminase were dissolved in a 20 mL PBS solution at 60 °C and at room temperature, respectively. A pre-gelled matrix composed of the gelatin and glutamine transaminase solution with a ratio of 10:1 was poured into a PDMS frame and kept at room temperature for two hours until the bubbles in the mixture were removed completely. After the pre-gelled matrix was completely congealed, a capillary glass tube was placed in the chip frame to extract the gelatin microchannel. Stainless-steel needles with a Teflon hose were inserted into both sides of the microchannel after removing the PDMS frame. HUVECs (Institute of Basic Medical Sciences, Chinese Academy of Medical Sciences Cell Resource Center, Beijing, China) were cultured in a culture flask for four days; then, the mixture of cells and cell culture media with a concentration of 106 cells/mL was injected into the microchannel. The microchannel chip with the HUVECs was cultured in the incubator under the condition of 5% CO2 and temperature of 37 °C until a complete endothelial monolayer was formed on the inner wall. Then, the mixture of human whole blood and NP suspension with a NP concentration of 109 particles/mL was infused into the microchannels for an hour at a flow rate of 100uL/h.

The morphology and activity of the cells were examined using calcein acetoxymethyl ester (calcein AM), fluorochrome 4'6-diamino-2-phenylindole (DAPI), and Alexa Fluor 488 phalloidin, which were purchased from Aladdin (Shanghai Aladdin Biochemical Technology Co., Ltd.). Calcein AM entered cells and green fluorescence was produced in the presence of intracellular esterase activity. The nuclei stained with DAPI exhibited blue fluorescence. The structure and distribution of cytoskeletons in the endothelial cells were determined though the green fluorescence produced by staining F-actin with phalloidin. Figure 2 shows the results examined under a laser scanning confocal microscope for the vessels with diameters of 100, 300 and 500 μm (Figure 2A, cross-sectional view). From the calcein AM staining results (Figure 2B), good cell activity was observed for each of the three microvessels, and nearly no red fluorescence was produced by the dead cells. The blue fluorescence images of DAPI-stained nuclei of the endothelial cells (Figure 2C) revealed that the cells were well dispersed and uniformly distributed on the inner wall. From the green fluorescence images of the phalloidin-stained F-actin cytoskeletons (Figure 2C), the actin filaments were found to be distributed uniformly, and the endothelial cells were closely connected with each other without superposition and gaps, indicating that one complete and annular monolayer of endothelial cells was formed on the inner wall. The barrier function of the

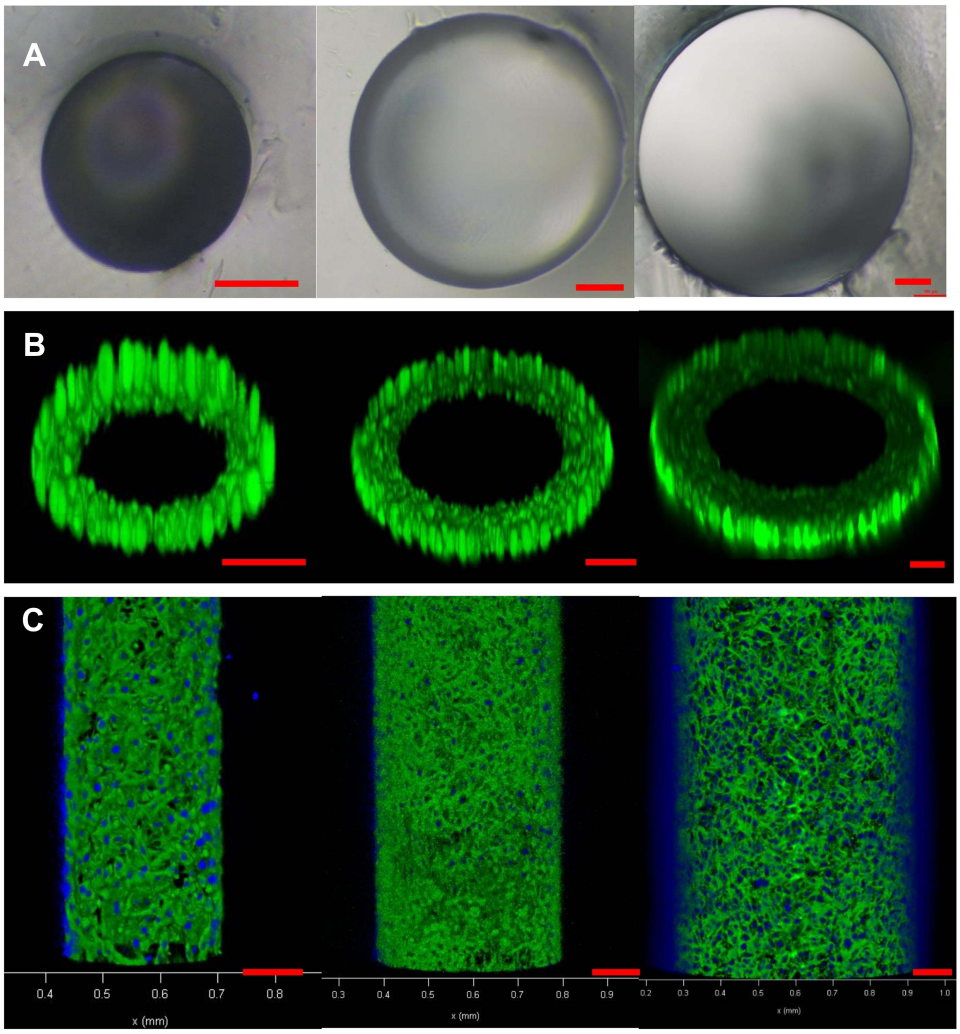

Figure 2 Fluorescence microscopic images of stained endothelial cells in microvessels with different diameters (100, 300 and 500 μm): (**A**) cross-section of gelatin-based microvessels, fluorescences of live endothelial cells stained with (**B**) calcein and (**C**) DAPI and Alexa Fluor 488 phalloidin. One complete and annular monolayer of live endothelial cells was observed on the inner wall.

blood vessel walls was effectively simulated, and the good biocompatibility and permeability of gelatin ensured the oxygen and nutrient transport in the microvessels. Therefore, this method can be applied for the construction of micro-scale blood vessels with good cell activity and can provide a good experimental basis for the study of NP transport and adhesion.

NPs and Characterization

Figures 3A–C show the TEM images of the gold NPs with different shapes (spherical and star-shaped NPs with 100 nm diameter, nanorod with 25 nm diameter and 102 nm length), which were purchased from Creative Diagnostics (Shirley, USA). Carboxyl gold NPs with a PEG3000 linker were citrate-stabilized and supplied in USP-grade purified water with high monodispersity and temperature stability and without aggregation. The pH of the NP suspension was measured with a pH meter (Fisher Scientific Accumet AP61, USA), and the value was approximately 7.2.

In this study, to investigate the NP adhesion behavior under the influence of receptor-ligand interaction in active-targeting drug delivery, the NPs were modified with RGD peptides on the surfaces for mutual recognition with the integrin αVβ3 expressed highly on the surface of HUVECs. A mixture of 3-dimethylaminopropyl-3-ethylcarbodiimide hydrochloride (EDC, purchased from Aladdin, China) and N-hydroxy succinimide (NHC, purchased from Aladdin, China) was prepared with an EDC concentration of 30 mg/mL and NHC concentration of 36 mg/mL. Then it was mixed

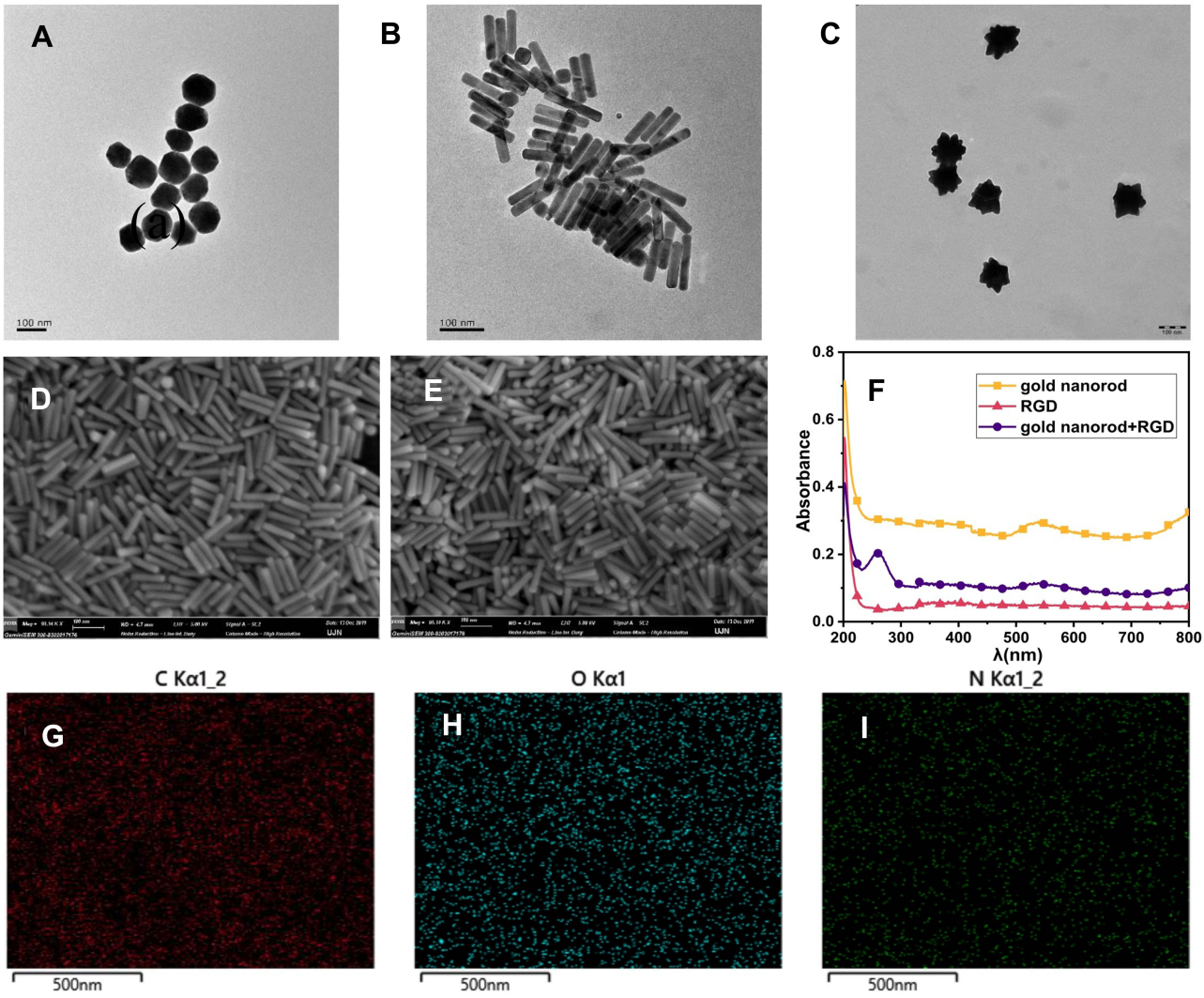

Figure 3 Characterization of NPs: (**A**–**C**) spherical, rod and star-shaped gold NPs, The diameter of the spherical and star-shaped NPs is 100nm, and the rod-shaped NPs have a 25nm diameter and a 102nm length, (**D**–**G**) SEM images and the ultraviolet absorption spectrum of rod gold NPs before and after RGD modification, the 258nm peak indicated the formation of amide groups, (**G**–**I**) elemental analysis after RGD modification.

with the NP suspension. After removing the supernatant of the mixture added with 1 mL phosphate-buffered saline (PBS) solution, the remaining solution and the RGD solution of 1mg/mL were mixed. The mixed solution was centrifuged and kept for 2–4 hours, and the RGD-coated NP solution was prepared after removing the supernatant.

Figures 3D–F show the SEM images and the ultraviolet absorption spectrum of rod gold NPs before and after RGD modification. The absorption peak of amide group appeared in the ultraviolet region after the nanorods was modified with RGD, due to the formation of amide groups caused by the amidation reaction between the amino group on RGD and the carboxyl group on the gold nanorod surface. Comparison of Figure 3D with Figure 3E revealed that a membrane layer was formed on the surface of the gold nanorod after the RGD modification. The results of X-ray dispersive spectroscopic analysis (Figure 3G–I) show that the three major elements of RGD (C, O and N) were uniformly distributed on the surface of gold nanorods, indicating that the surfaces of NPs were modified with RGD.

Atomic Force Microscopy Measurements

Atomic force microscopy (AFM, MFP3D-Bio, Oxford Instruments, UK) was used to measure the RGD–integral αvβ3 interaction forces at different temperatures. The silicon AFM probes (k=0.2N/m, HQ-13-Au, Asylum Research) were functionalized using the dip-coating method, for which the AFM tips were immersed into the RGD peptide solutions, and

then dried in air. The immersion process was repeated at least five times to ensure that the RGD peptide could cover the surface of the AFM tips. After the functionalized probes were dried for at least 24 h, the sensitivity of the photodetector was calibrated using an empty petri dish, and the spring constant of the AFM tips was obtained via thermal tuning. The force distance was set to 7 μm, and the trigger point was set to 0.5 nN. The force-distance and scan rate were set to 2 μm and 0.5 Hz, respectively. Three regions on the substrate were randomly selected, and 6–8 cells within each region could be observed in the visual field. By performing 50 individual measurements of the interaction force in each region, a total of 150 force curves were obtained for each case.

Temperature Control

A solid-state plug-in stage (Pecon stage insert, PECON, Germany) made from a piece of aluminium was applied to stably cool and heat the artificial blood vessel system with high temperature stability and uniform distribution. The vessel system was firmly fixed in the stage, which was placed on an upright microscope for on-site living cell imaging. The temperature was controlled by the circulating liquid from a thermostatic water bath (CD-600F, JULABO, Germany) connected to the plug-in stage. In consideration of the activity of the endothelium cells cultured in the vessels, five temperature points (25°C, 37°C, 39°C, 41°C, and 43°C) were selected to investigate the effect of temperature on NP transport and adhesion in the microvessels.

Analysis of NP Adhesion

The ICP-MS method was employed for the quantitative analysis of NP adhesion in the artificial vessels. All the glass containers were soaked in aqua regia for at least 12 h, and rinsed with ultra-pure water (18.3 MΩ·cm) and dried in an oven at 110 °C for 2 min. To ensure that the measurements were performed under the same conditions, the concentrations of different NPs in the suspensions injected into the vessel were all set to approximately 109 particles/mL. After 1 hr of perfusion with the mixture of the whole blood and NP suspension, the artificial blood vessel sample was dissolved in aqua regia until no solid residue remained. Then, the mixed solution was heated at 120 °C until it completely evaporated. During the process of evaporation, a hydrogen peroxide solution was continuously added dropwise to the mixture to remove the high-concentration HNO3 from the mixed solution, thereby avoiding the damage to the instrument and samples. Afterwards, the obtained solid powder after evaporation was dissolved in a container by using 8 mL of 2% diluted nitric acid for ICP-MS testing (NexION 300X, Perkin Elmer, USA).

Results and Discussion

Effects of NP Properties

Gold NPs with the same ligand density but different shapes and sizes (ie, sphere, rod, and star; nanorod: 10×41 nm, 25×41 nm, and 40×208 nm) were injected into the artificial blood vessels as nanofluids having the same NP capacity. The experimental results are shown in Figure 4A. The NP adhesion on the vessel wall was enhanced by the decrease in NP size because the Brownian force acting on small NPs is larger than that acting on large NPs, leading to a highly vigorous random movement and increased margination probability. In addition, the vigorous movement of small NPs causes great turbulence of blood flow and large drag force with highly varied magnitude and direction, which can also increase the probability of the NPs moving towards the vessel wall and subsequently improve NP adhesion.

As shown in Figure 4A, the number of adhered rod NPs was larger than that of the star-shaped NPs, followed by the spherical NPs. A possible reason is that non-spherical NPs can lead to the occurrence of greater disturbance in the flow field compared with spherical NPs. This condition can make the fluid drag forces acting on non-spherical NPs change drastically and enable the NPs to move irregularly and intensively. Accordingly, the NP margination probability is increased, and NP adhesion is enhanced. The difference in adhesion to the wall between the rod and star-shaped NPs might depend on NP irregularity related to the NP shape and dimension ratio. Moreover, the surface areas of the NPs with an irregular structure are larger than those of spherical NPs, which means that more ligands might be modified on the surfaces of irregular NPs and that more ligand–receptor pairs would be formed. An improved ligand–receptor interaction can also prevent NP detachment from vessel walls once the NPs adhere to the vessel surface. Based on the

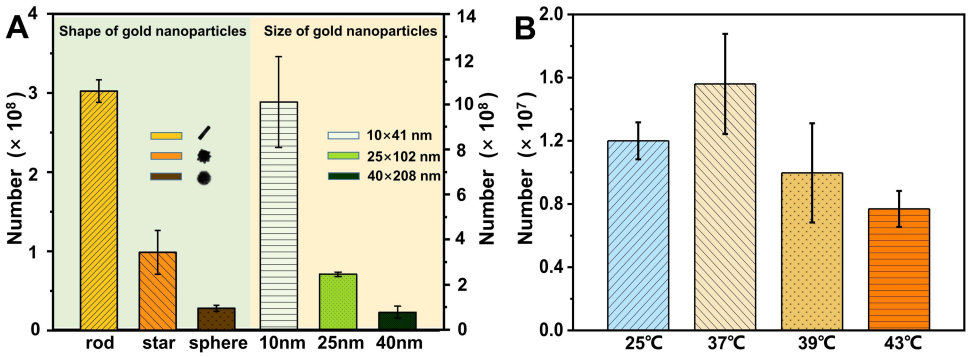

Figure 4 The numbers of adhered NPs under conditions of: (**A**) different shapes and sizes at the temperature of 37°C, and (**B**) different temperatures for the rod-shaped NPs. The maximal number of adhered NPs was reached at 37 °C for the rod-shaped NPs having a size of 10×41nm.

results mentioned above, the 10×41 nm rod-shaped NPs were used to explore the effect of temperature on NP adhesion in the artificial blood vessel. Figure 4B shows the experimental results, which will be discussed in detail in Effect of Temperature on NP Adhesion and Ligand–Receptor Interaction.

Changes in Cell Morphology and Activity with Temperature

To analyze the influence of temperature variation within a reasonable range on NP adhesion, the temperatures of the stage (Figure 1) and pumping pipes were controlled at 25 °C, 37 °C, 39 °C, 41 °C, and 43 °C by using a thermostatic water bath. Firstly, gelatin-based artificial vessels with endothelial cells on the inner wall were cultured statically and under continuous perfusion at controlled temperatures for 1 h. Secondly, the endothelial cells were stained with calcein AM, propidium iodide (PI) and phalloidin. PI binds to DNA in the nucleus of dead cells to produce red fluorescence and is often used to measure cell activity. Figure 5A shows the changes in cell activity and morphology after 1 h of static culture.

As shown in Figures 5B and C, the strongest green fluorescence produced by calcein AM staining was observed at 37 °C, and almost no cell death was detected (Figure 5A). The cells with a polygonal outer shape spread out completely with an obvious microfilament structure (Figures 5B and C). As the temperature increased, the cells and their pseudopodia gradually retracted, tending to become round in shape and leading to increased gaps between the cells. Cell activity was gradually attenuated according to the decreased fluorescence intensity and the red fluorescence indicating dead cells. The increase in temperature led to an increase in the number of dead cells. Similarly, the cells also had a tendency to shrink and become round in shape, and the activity of the cells decreased obviously as the temperature decreased. The changes in cell activity and morphology at 25 °C were smaller than those at 39 °C, 41 °C, and 43 °C, leading to the conclusions that the effect of low temperature was less than that of high temperature and the cell activity was the best at 37 °C.

Furthermore, the effect of temperature on cells in the continuous perfusion culture was analyzed using calcein AM, phalloidin and DAPI staining. Figures 6A and B show the results of calcein AM staining before and after 1 h of continuous blood perfusion. Figure 6C presents the patterns of the F-actin of endothelial cells stained with phalloidin and nuclear DNA stained with DAPI. As can be seen in Figure 6C, much more blue fluorescent spots at 37 °C can be observed compared with those at 25 °C and 41 °C, and the intensities of the blue and green fluorescences at 37 °C were also stronger than the latter. The findings show that the endothelial cells at 37 °C can completely spread out and closely connected with each other compared with those at 25 °C and 41 °C, indicating that the cells displayed good activity and could adhere well to the surface of the inner vessel wall even under the condition of continuous perfusion. The influence of blood flow on cell morphology was not as obvious as that under the static culture conditions, and the cells did not obviously elongate; their axis was aligned with the flow direction, as can be found in literature.[51] A possible reason is that continuous blood perfusion was performed for only one hour in this study due to the consideration of cell activity under high temperatures. Some cells gradually shrank from a full spreading shape to a round shape as the temperature increased or decreased, which was similar to the phenomenon observed under the static culture condition. However, some cells were detached from the inner wall of the vessel at 43 °C under the

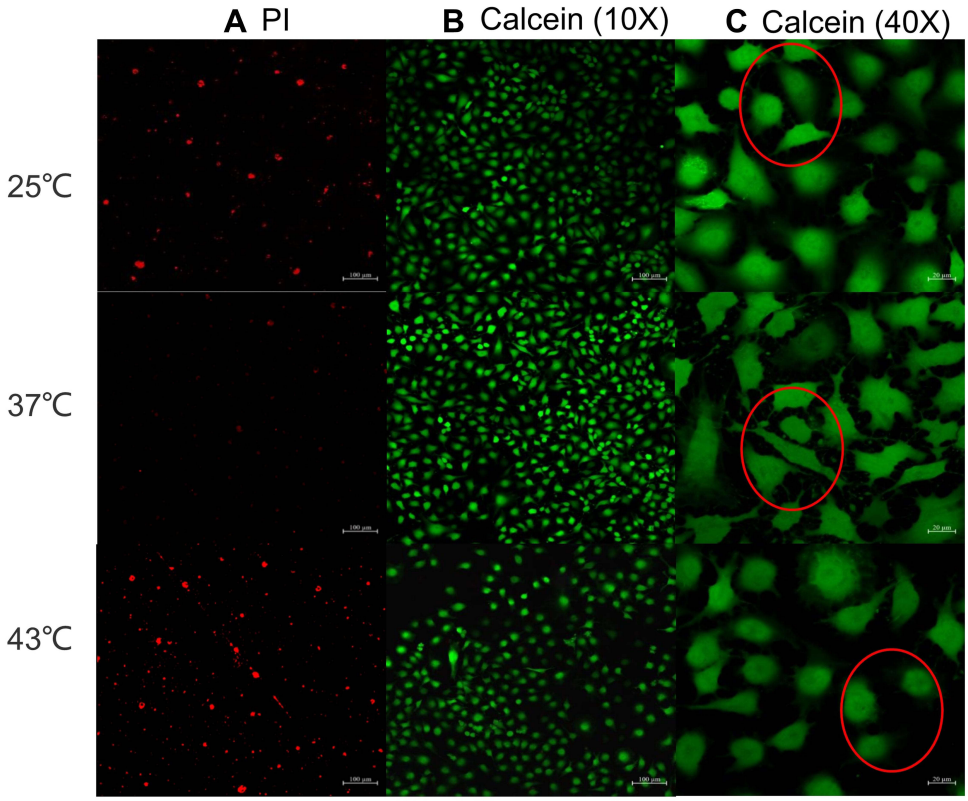

Figure 5 Effect of temperature on the cells in static culture: (**A**) images of nuclear PI staining, and the fluorescence intensity was the strongest at 43°C, (**B** and **C**) images of Calcein-AM staining with a magnification of 10X and 40X. The cell activity was the best at 37°C.

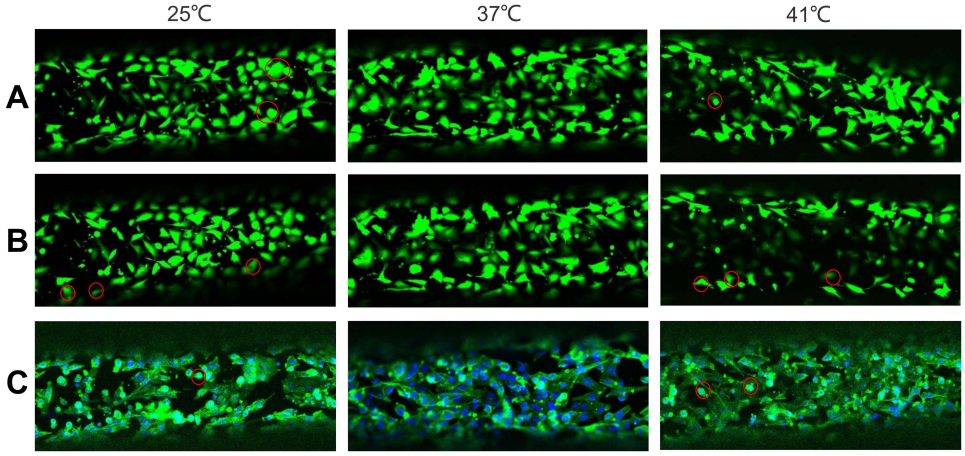

Figure 6 Effect of temperature on the cells in continuous perfusion culture: (**A** and **B**) fluorescence staining with calcein AM before and after 1 h of continuous blood perfusion (100μL/h), and (**C**) fluorescence staining with phalloidin and DAPI after 1 h of continuous blood perfusion (100μL/h).

action of blood flow possibly because the degeneration of fibrin and depolymerization of the cytoskeleton caused by temperature variation weakened the adhesion of cells on the growth surface.

Effect of Temperature on NP Adhesion and Ligand–Receptor Interaction

After 1 h of continuous perfusion of the mixture of the whole blood and NP suspension in the vessel, the number of 100 nm gold NPs adhered to the vessel was measured by ICP-MS at 25°C, 37°C, 39°C, and 43°C. As shown in Figure 4B, the mean number of adhered NPs was 1.20×10^7, 1.56×10^7, 9.97×10^6, and 7.69×10^6. The maximum was reached at 37°C and decreased

with the increase or decrease in temperature. The particle adhesion at the temperature of 25°C was better than that at 39°C and reached the minimum at 43°C. Our previous simulation work[50] showed that an increase in temperature leads to an increase in the number of NPs attached to the vessel wall when the influence of temperature on the binding of the ligands on NPs to the receptors of endothelial cells is ignored. The reason is that the drag force acting on the particles and the Brownian movement of the particles change greatly with the increase in temperature, leading to a high probability of NP margination to the vessel wall for adhesion. To explain the experimental results, the ligand–receptor interaction forces between the RGD peptide and integral αvβ3 on the cell surface were quantitatively determined by AFM under different temperature conditions.

The control group in the experimental measurements used bare tips, and the experimental group employed RGD-coated tips. Figures 7A and B show the distributions of the interaction forces of the two groups at different temperatures. The mean interaction forces of the control group (Figure 7C) at 25°C, 37°C, 39°C, and 43°C were 0.5±0.3, 0.6±0.4, 0.4±0.2, and 0.3±0.2nN, respectively, and those of the experimental group were 2.5±0.5, 3.2±0.8, 2.2±0.5, and 0.6±0.4nN, respectively. The ligand–receptor interaction decreased when the temperature was lower or higher than 37 °C maybe because of the denaturation of the receptor integral αvβ3. In addition, the effect of low temperature was less than that of high temperature. The endothelial cells at different temperatures were also imaged via AFM (Figure 7D). As observed in previous experiments, the endothelial cells grew well at 37°C. The cytoskeleton fibers were clearly visible, but the fibers and pseudopodia disappeared and the cells shrunk to a round shape when the temperature increased or decreased, leading to an increase in intercellular space.

Evidently, thermal or cold stimulation can lead to damage in the microfilament structure of endothelial cells, an increase in intercellular space, and an increase in the proportion of dead cells on the growth surface of the inner vessel wall. These changes can result in decrements in the number of binding receptors and the ligand-binding domain, thus

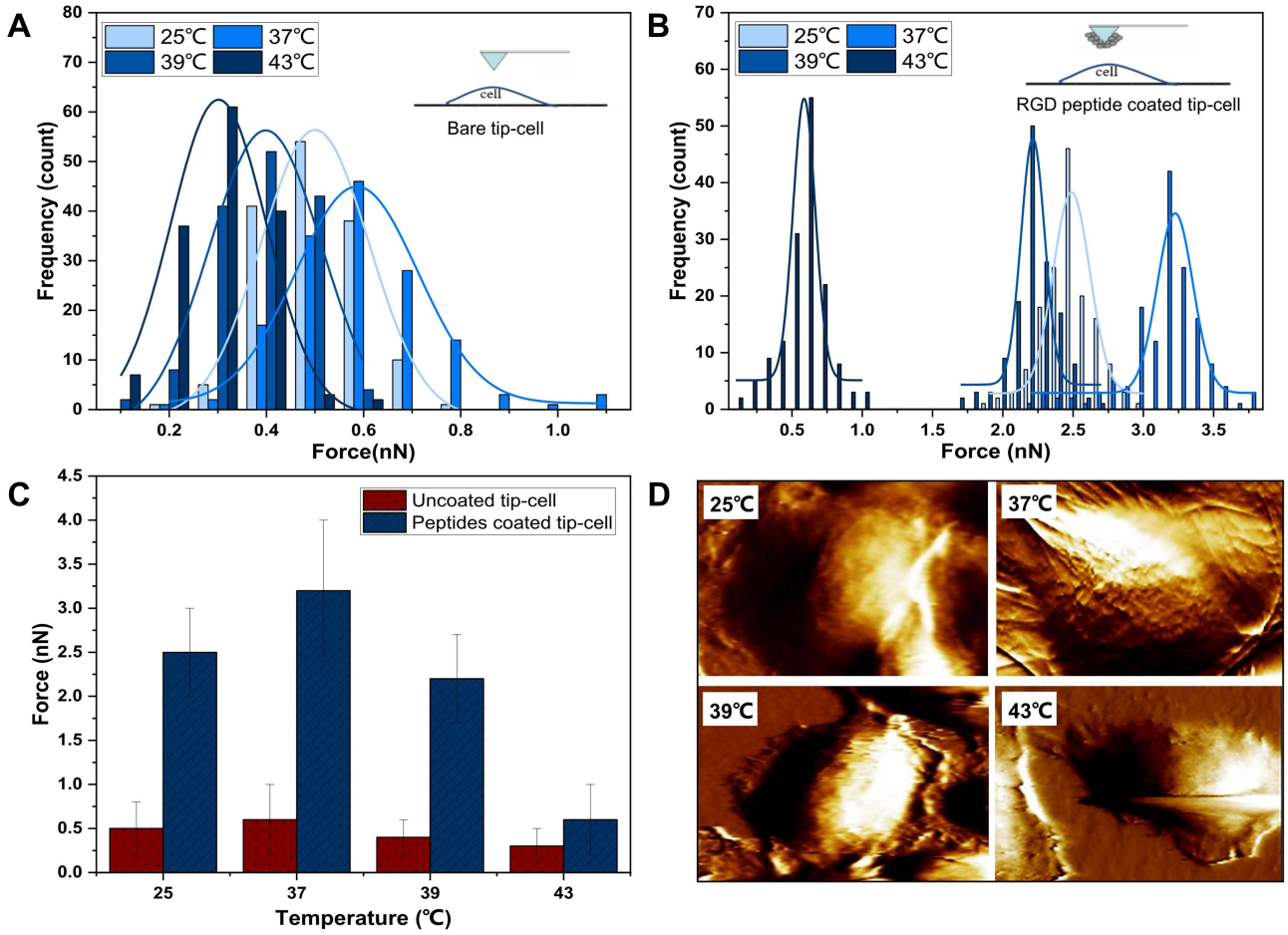

Figure 7 AFM measurement of receptor–ligand interaction under different temperatures: (**A** and **B**) statistical analysis of 150 measurements of the interactions of the cell-bare and cell-coated tips, (**C**) measurement results of receptor–ligand interaction force, and (**D**) change in cell morphology under different temperatures.

lowering the probability of the binding of the ligands to the receptors on the endothelial cell surfaces. Moreover, when the temperature was lower or higher than 37 °C, the activity of the cells was decreased and the proteins on the surface of the cell membrane were denatured and inactivated gradually, which weakened the binding of integral receptors to ligands on the NP surfaces. The two factors can explain the reduced number of NPs attached to the vascular wall when the temperature deviated from 37 °C.

Conclusion

We developed a gelatin-based artificial blood vessel system with good biocompatibility and permeability that enable the good growth of endothelial cells on the inner surface of the vessel wall under static and perfusion culture conditions. The ligand-coated NPs with a small particle size and non-spherical shape exhibited good adhesion in the blood vessel system, demonstrating that the developed system can be used feasibly and reliably to investigate the transport and adhesion behaviors of different NPs in microvessels. The number of NPs attached to the vascular wall was the largest at the temperature of 37°C Cell activity and morphology were sensitive to the environmental temperature, and the cells in the perfusion culture detached from the wall under the action of fluid shear force at high temperatures. When the temperature was higher or lower than 37°C, the decrease in cell activity and the contraction of the cytoskeleton structure reduced the number of attached NPs due to the weakened ligand–receptor interaction and the decrease in the ligand–receptor binding domain. The corresponding change at 25°C was less than that at 39°C, indicating that the effect of low temperatures on the cells was less than that of high temperatures. To improve NP adhesion in target tissues under influence of temperature variations caused by the action of external fields, a possible strategy is to identify the specific ligand-binding sites of the integral receptor that are not considerably influenced by temperature changes. Then, the ligand may be redesigned to enhance the ligand–receptor interaction at these ligand–binding sites. A multi-target drug delivery system that employs binding receptors that are minimally susceptible to temperature variations is also a potential solution.

Acknowledgment

This work was supported by the National Natural Science Foundation of China for financial support (Grant No.51890891 and No.51890894) and Scientific and Technological Innovation Foundation of Shunde Graduate School, USTB (Grant No. BK20AE002).

Disclosure

The authors report no conflicts of interest in this work.

References

1. Barreto JA, O'Malley W, Kubeil M, Graham B, Stephan H, Spiccia L. Cancer research: nanomaterials: applications in cancer imaging and therapy. *Adv Mater*. 2011;23(12):H2–H2. doi:10.1002/adma.201190041
2. Uribe madrid SI, Pal U, Kang YS, Kim J, Kwon H, Kim J. Fabrication of Fe3O4@ mSiO2 core-shell composite nanoparticles for drug delivery applications. *Nanoscale Res Lett*. 2015;10(1):1–8. doi:10.1186/s11671-015-0920-5
3. Xu H, Fan M, Elhissi AMA, et al. PEGylated graphene oxide for tumor-targeted delivery of paclitaxel. *Nanomedicine*. 2015;10(8):1247–1262. doi:10.2217/nnm.14.233
4. Casi G, Neri D. Antibody–drug conjugates and small molecule–drug conjugates: opportunities and challenges for the development of selective anticancer cytotoxic agents: miniperspective. *J Med Chem*. 2015;58(22):8751–8761. doi:10.1021/acs.jmedchem.5b00457
5. Muhamad N, Plengsuriyakarn T, Na-Bangchang K. Application of active targeting nanoparticle delivery system for chemotherapeutic drugs and traditional/herbal medicines in cancer therapy: a systematic review. *Int J Nanomedicine*. 2018;13:3921. doi:10.2147/IJN.S165210
6. Marques AC, Costa PJ, Velho S, Amaral M. Functionalizing nanoparticles with cancer-targeting antibodies: a comparison of strategies. *J Control Release*. 2020;320:180–200. doi:10.1016/j.jconrel.2020.01.035
7. Wu M, Huang S. Magnetic nanoparticles in cancer diagnosis, drug delivery and treatment. *Mol Clin Oncol*. 2017;7(5):738–746. doi:10.3892/mco.2017.1399
8. Feng Q, Zhang Y, Zhang W, et al. Programmed near-infrared light-responsive drug delivery system for combined magnetic tumor-targeting magnetic resonance imaging and chemo-phototherapy. *Acta Biomater*. 2017;49:402–413. doi:10.1016/j.actbio.2016.11.035
9. Zhao Z, Ukidve A, Krishnan V, Mitragotri S. Effect of physicochemical and surface properties on in vivo fate of drug nanocarriers. *Adv Drug Deliv Rev*. 2019;143:3–21. doi:10.1016/j.addr.2019.01.002
10. Mitchell MJ, Billingsley MM, Haley RM, Marissa EW, Nicholas AP, Robert L. Engineering precision nanoparticles for drug delivery. *Nat Rev Drug Discov*. 2021;20(2):101–124. doi:10.1038/s41573-020-0090-8

11. Zhang S, Langer R, Traverso G. Nanoparticulate drug delivery systems targeting inflammation for treatment of inflammatory bowel disease. *Nano Today*. 2017;16:82–96. doi:10.1016/j.nantod.2017.08.006
12. Decuzzi P, Gentile F, Granaldi A, et al. Flow chamber analysis of size effects in the adhesion of spherical particles. *Int J Nanomedicine*. 2007;2 (4):689. PMCID: PMC2676800.
13. Zhao N, Wei Y, Sun N, et al. Controlled synthesis of gold nanobelts and nanocombs in aqueous mixed surfactant solutions. *Langmuir*. 2008;24 (3):991–998. doi:10.1021/la702848x
14. Jurney P, Agarwal R, Singh V, Roy K, Sreenivasan S, Shi L. Size-dependent nanoparticle margination and adhesion propensity in a microchannel. *J Nanotechnol Eng Med*. 2013;4(3):031002. doi:10.1115/1.4025609
15. Gentile F, Curcio A, Indolfi C, Ferrari M, Decuzzi P. The margination propensity of spherical particles for vascular targeting in the microcirculation. *J Nanobiotechnology*. 2008;6(1):1–9. doi:10.1186/1477-3155-6-9
16. Toy R, Hayden E, Shoup C, Baskaran H, Karathanasis E. The effects of particle size, density and shape on margination of nanoparticles in microcirculation. *Nanotechnology*. 2011;22(11):115101. doi:10.1088/0957-4484/22/11/115101
17. Hao N, Li L, Zhang Q, et al. The shape effect of PEGylated mesoporous silica nanoparticles on cellular uptake pathway in Hela cells. *Microporous Mesoporous Mater*. 2012;162:14–23. doi:10.1016/j.micromeso.2012.05.040
18. Hao N, Liu H, Li L, Chen D, Li L, Tang F. In vitro degradation behavior of silica nanoparticles under physiological conditions. *J Nanosci Nanotechnol*. 2012;12(8):6346–6354. doi:10.1166/jnn.2012.6199
19. Gratton SEA, Ropp PA, Pohlhaus PD, et al. The effect of particle design on cellular internalization pathways. *Proc Natl Acad Sci*. 2008;105 (33):11613–11618. doi:10.1073/pnas.0801763105
20. Cong VT, Gaus K, Tilley RD, Justin GJ. Rod-shaped mesoporous silica nanoparticles for nanomedicine: recent progress and perspectives. *Expert Opin Drug Deliv*. 2018;15(9):881–892. doi:10.1080/17425247.2018.1517748
21. Geng YAN, Dalhaimer P, Cai S, et al. Shape effects of filaments versus spherical particles in flow and drug delivery. *Nat Nanotechnol*. 2007;2 (4):249–255. doi:10.1038/nnano.2007.70
22. Gentile F, Chiappini C, Fine D, et al. The effect of shape on the margination dynamics of non-neutrally buoyant particles in two-dimensional shear flows. *J Biomech*. 2008;41(10):2312–2318. doi:10.1016/j.jbiomech.2008.03.021
23. Souri M, Soltani M, Kashkooli FM, Shahvandi MK. Engineered strategies to enhance tumor penetration of drug-loaded nanoparticles. *J Control Release*. 2022;341:227–246. doi:10.1016/j.jconrel.2021.11.024
24. Souri M, Soltani M, Kashkooli FM, et al. Towards principled design of cancer nanomedicine to accelerate clinical translation. *Materials Today Bio*. 2022;13:100208. doi:10.1016/j.mtbio.2022.100208
25. Brown SD, Nativo P, Smith JA, et al. Gold nanoparticles for the improved anticancer drug delivery of the active component of oxaliplatin. *J Am Chem Soc*. 2010;132(13):4678–4684. doi:10.1021/ja908117a
26. Khan AK, Rashid R, Murtaza G, et al. Gold nanoparticles: synthesis and applications in drug delivery. *Trop J Pharm Res*. 2014;13(7):1169–1177. doi:10.4314/tjpr.v13i7.23
27. Singh M, Singh S, Prasad S, Gambhir I. Nanotechnology in medicine and antibacterial effect of silver nanoparticles. *Dig J Nanomater Biostruct*. 2008;3:115–122. HERO ID: 2575536.
28. Shrivastava S, Bera T, Roy A, Singh G, Ramachandrarao P, Dash D. Characterization of enhanced antibacterial effects of novel silver nanoparticles. *Nanotechnology*. 2007;18(22):225103. doi:10.1088/0957-4484/18/22/225103
29. Aoudia M, Cheng G, Kennedy VO, Kenney ME, Rodgers MA. Synthesis of a series of octabutoxy-and octabutoxybenzophthalocyanines and photophysical properties of two members of the series. *J Am Chem Soc*. 1997;119(26):6029–6039. doi:10.1021/ja963702q
30. Anglin EJ, Cheng L, Freeman WR, Sailor MJ. Porous silicon in drug delivery devices and materials. *Adv Drug Deliv Rev*. 2008;60(11):1266–1277. doi:10.1016/j.addr.2008.03.017
31. Malam Y, Loizidou M, Seifalian AM. Liposomes and nanoparticles: nanosized vehicles for drug delivery in cancer. *Trends Pharmacol Sci*. 2009;30 (11):592–599. doi:10.1016/j.tips.2009.08.004
32. Forier K, Raemdonck K, De Smedt SC, Demeester J, Coenye T, Braeckmans K. Lipid and polymer nanoparticles for drug delivery to bacterial biofilms. *J Control Release*. 2014;190:607–623. doi:10.1016/j.jconrel.2014.03.055
33. Needham D, Dewhirst MW. The development and testing of a new temperature-sensitive drug delivery system for the treatment of solid tumors. *Adv Drug Deliv Rev*. 2001;53(3):285–305. doi:10.1016/S0169-409X(01)00233-2
34. Qiu Y, Tong S, Zhang L, et al. Magnetic forces enable controlled drug delivery by disrupting endothelial cell-cell junctions. *Nat Commun*. 2017;8 (1):1–10. doi:10.1038/ncomms15594
35. Deckers R, Rome C, Moonen CTW. The role of ultrasound and magnetic resonance in local drug delivery. *J Magn Reson Imaging*. 2008;27 (2):400–409. doi:10.1002/jmri.21272
36. Patel T, Zhou J, Piepmeier JM, Saltzman WM. Polymeric nanoparticles for drug delivery to the central nervous system. *Adv Drug Deliv Rev*. 2012;64(7):701–705. doi:10.1016/j.addr.2011.12.006
37. Muzykantov VR. Biomedical aspects of targeted delivery of drugs to pulmonary endothelium. *Expert Opin Drug Deliv*. 2005;2(5):909–926. doi:10.1517/17425247.2.5.909
38. Hida K, Maishi N, Sakurai Y, Hida Y, Harashima H. Heterogeneity of tumor endothelial cells and drug delivery. *Adv Drug Deliv Rev*. 2016;99:140–147. doi:10.1016/j.addr.2015.11.008
39. Dziubla TD, Shuvaev VV, Hong NK, et al. Endothelial targeting of semi-permeable polymer nanocarriers for enzyme therapies. *Biomaterials*. 2008;29(2):215–227. doi:10.1016/j.biomaterials.2007.09.023
40. Haun JB, Hammer DA. Quantifying nanoparticle adhesion mediated by specific molecular interactions. *Langmuir*. 2008;24(16):8821–8832. doi:10.1021/la8005844
41. Zhen Z, Tang W, Chen H, et al. RGD-modified apoferritin nanoparticles for efficient drug delivery to tumors. *ACS nano*. 2013;7(6):4830–4837. doi:10.1021/nn305791q
42. Millard M, Odde S, Neamati N. integral targeted therapeutics. *Theranostics*. 2011;1:154. doi:10.7150/thno/v01p0154
43. Huang HS, Hainfeld JF. Intravenous magnetic nanoparticle cancer hyperthermia. *Int J Nanomedicine*. 2013;8:2521. doi:10.2147/IJN.S43770
44. Pearce JA, Cook JR, Emelianov SY. Ferrimagnetic nanoparticles enhance microwave heating for tumor hyperthermia therapy[C]//2010 Annual International Conference of the IEEE Engineering in Medicine and Biology. *IEEE*. 2010;2751–2754. doi:10.1109/IEMBS.2010.5626583

45. Tamarov KP, Osminkina LA, Zinovyev SV, et al. Radio frequency radiation-induced hyperthermia using Si nanoparticle-based sensitizers for mild cancer therapy. *Sci Rep*. 2014;4(1):1–7. doi:10.1038/srep07034
46. O'Neal DP, Hirsch LR, Halas NJ, Payne JD, West JL. Photo-thermal tumor ablation in mice using near infrared-absorbing nanoparticles. *Cancer Lett*. 2004;209(2):171–176. doi:10.1016/j.canlet.2004.02.004
47. Nance E, Timbie K, Miller GW, et al. Non-invasive delivery of stealth, brain-penetrating nanoparticles across the blood-brain barrier using MRI-guided focused ultrasound. *J Control Release*. 2014;189:123–132. doi:10.1016/j.jconrel.2014.06.031
48. Peng X, Recchia FA, Byrne BJ, et al. In vitro system to study realistic pulsatile flow and stretch signaling in cultured vascular cells. *Am J Physiol Cell Physiol*. 2000;279(3):C797–C805. doi:10.1152/ajpcell.2000.279.3.C797
49. Wong K, Chan J, Kamm RD, Tien J. Microfluidic models of vascular functions. *Annu Rev Biomed Eng*. 2012;14(1):205–230. doi:10.1146/annurev-bioeng-071811-150052
50. Yue K, You Y, Yang C, Niu Y, Zhang X. Numerical simulation of transport and adhesion of thermogenic nano-carriers in microvessels. *Soft Matter*. 2020;16(45):10345–10357. doi:10.1039/D0SM01448F
51. Mondrinos MJ, Yi Y, Wu N, Ding X, Huh D. Native extracellular matrix-derived semipermeable, optically transparent, and inexpensive membrane inserts for microfluidic cell culture. *Lab Chip*. 2017;17(18):3146–3158. doi:10.1039/C7LC00317J